Marine Structures 78 (2021) 102972

Contents lists available at ScienceDirect

Marine Structures

journal homepage: http://www.elsevier.com/locate/marstruc

Seismic response of subsea structures on caissons and mudmats due to liquefaction

Pourya Kazemi Esfeh [a], Laura Govoni [a], Amir M. Kaynia [b,c,*]

[a] Department of Civil, Chemical, Environmental, and Materials Engineering University of Bologna (UNIBO), Italy
[b] Norwegian Geotechnical Institute (NGI), Norway
[c] Norwegian University of Science and Technology (NTNU), Trondheim, Norway

ARTICLE INFO

Keywords:
Liquefaction
Seismic analysis
Caisson
Mudmat
Subsea structures
SANISAND constitutive Model

ABSTRACT

This paper presents a numerical study to investigate the seismic behavior of mudmat and caisson foundations supporting subsea structures, such as manifolds, in liquefiable sand. In seismic areas, substantial earthquake loads can be imparted to subsea structures during ground shaking, threatening their stability. In particular, soil liquefaction in sandy soil arising from strong ground motions could significantly influence the performance of subsea structures founded on liquefiable sand. The results of this study can provide a better understanding of the response of subsea manifolds in liquefiable soil during and after the earthquake. Three-dimensional, non-linear, dynamic analyses are performed using a finite difference scheme, and the ability of the model to reproduce the site response of a saturated sand deposit is assessed using the results of available centrifuge data. This study includes six computational models representing manifolds with different sizes and weights supported by caissons and mudmats in shallow and deep liquefiable sand subjected to moderate and strong earthquake shakings. The response is evaluated in terms of excess pore water pressure generated in the soil medium and displacements of the subsea foundation during and after the shaking. The results show that manifolds may experience considerable movement during liquefaction and post-liquefaction settlements. In addition, depending on the characteristics of the seismic motion and structural system, the manifold could also experience large tilting.

1. Introduction

Subsea production systems include a variety of structures and facilities varying in size and weight from relatively heavy wellhead trees to large manifolds and templates. The type and size of foundations for subsea facilities could widely vary depending on the size of the structure, soil conditions, and available installation techniques [1].

Mudmats are the most common foundations for subsea production facilities hereinafter referred to as subsea structures. A mudmat is a steel plate often with short peripheral and, in some cases, internal skirts to provide a better bond to the seabed and easier installation (Fig. 1). They have typically a width-to-length ratio of 0.2–1 and the length of skirt is generally less than 0.1 of the mudmat's width [7]. Mudmats are often perforated to facilitate their installation and removal [2]. This type of foundation is preferred to other types due to its easier installation under the self-weight of foundation and structure [10]. For heavier and larger subsea

* Corresponding author.Norwegian University of Science and Technology (NTNU), Trondheim, Norway.
E-mail addresses: pooria.kazemi@studio.unibo.it (P.K. Esfeh), l.govoni@unibo.it (L. Govoni), amir.m.kaynia@ngi.no (A.M. Kaynia).

https://doi.org/10.1016/j.marstruc.2021.102972
Received 10 August 2020; Received in revised form 24 November 2020; Accepted 9 February 2021
Available online 16 March 2021

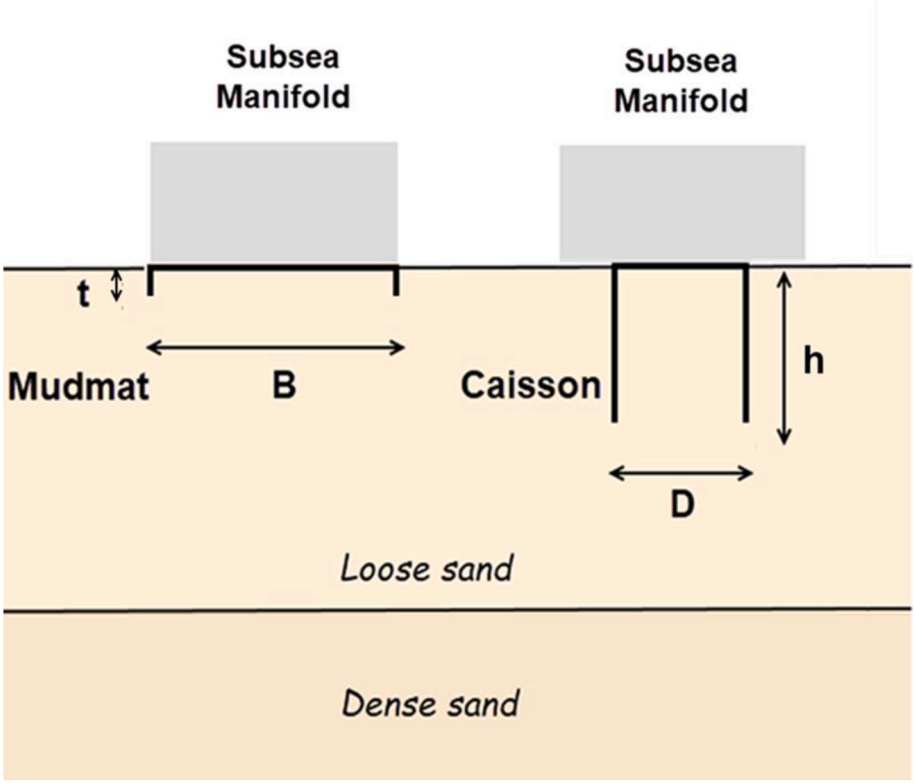

Fig. 1. Schematics of subsea manifolds founded on mudmat (left) and caisson (right).

structures, or when the seabed soil is very soft, suction caissons are commonly used as an alternative. A suction caisson is a steel cylinder open at the base and closed at the top with a lid (Fig. 1). This foundation type has been largely used in offshore practice since its first installation in the early '90s [3]. The caisson, first, penetrates the soil by self-weight, then a suction pressure is applied by pumping out the water trapped within the caisson to drive the foundation to its full depth. Caissons vary in size and slenderness depending on the soil and loading conditions. These two foundation types are referred to as subsea foundations in the following.

Subsea foundations are primarily subjected to structural loads, including the weight of the structure, and the operational loads associated with the piping. Depending on their point of action, these loads can produce moments and torsions on the foundation. Fluid drag and lift from waves and currents also may contribute to complex loading patterns, although their intensity is expected to be moderate in deep waters. Several studies have comprehensively reported on the monotonic plastic response of subsea foundations under multidirectional loading conditions (e.g. Refs. [4–10]).

In seismically active areas, substantial earthquake loads can act on subsea structures in addition to the loads described above. Furthermore, depending on the structural configurations, subsea foundations on liquefiable soil deposits could experience significant displacements and rotations during liquefaction compromising their safety and stability. Spools and pipelines lying on the seabed connect subsea facilities. These elements are relatively light and flexible and follow the movements of the structures at the two ends unless they are placed on slopes with possible downslope movements [11]. Therefore, large transitional displacements and rotations of the structure due to liquefaction could overstress these sensitive elements leading to severe consequences.

The research on the earthquake response of subsea foundations is rather limited, and, where available, mainly focused on soft clay deposits (e.g. Refs. [12,13]). Although several numerical studies have been devoted to the seismic response of offshore breakwaters (e.g. Refs. [14–18]), as well as the effects of liquefaction induced by waves and current actions on buried pipelines (e.g. Refs. [19,20]), the literature gap on the earthquake response of subsea foundations installed in liquefiable soils is apparent. The problem is, in fact, very complex, and intrinsically three-dimensional, and it is governed by the strong non-linearities of the soil-foundation interaction.

The present lack of information on the seismic behavior of subsea foundations in liquefaction-prone soils could give rise to uncertainties and design consequences; thus, a more critical assessment of this matter should be carried out in addition to routine procedures followed in design of these foundations. In most design cases, the foundation concept is just altered and a piled foundation is prescribed across the liquefiable soil layer with clear consequences on the capital expenditure. In more demanding projects with complex structures (e.g. Refs. [21,22]), current procedures involve the use of simplified, although usually not straightforward, solutions that make use of one-dimensional models to predict the seismic stress history of a soil element, with separate evaluation of pore water pressure accumulation through analytical approaches.

Numerous studies have focused on evaluating the earthquake response of shallow and deep foundations as well as seismic soil-

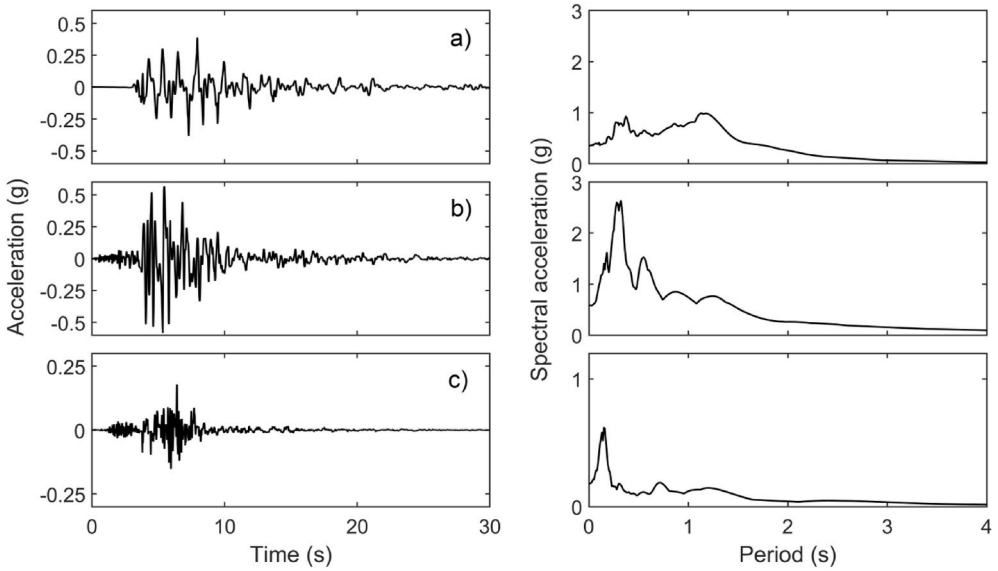

Fig. 2. Acceleration time histories and corresponding acceleration spectra for horizontal component of a) Kobe and b) Northridge-Newhall earthquakes and c) vertical component of Kobe earthquake.

structure interaction (e.g. Refs. [23–29]); nonetheless, only a few of these studies correspond to the dynamic response of subsea foundations in particular. Wolf [23] proposed simple physical models (spring-dashpot-mass models) together with simple one-dimensional wave patterns in the horizontal plane to better understand the dynamics of surface, embedded and pile foundations and soil-structure interaction. The solution has been extended to underwater foundations (e.g. Ref. [30]) using rigorous analytical solutions of wave propagation underwater ([31]). Liingaard [24] conducted extensive research on the frequency-dependence of the dynamic stiffness of suction caissons for offshore wind turbines using simple models suggested in Ref. [23]. Brandt [25] and Stensløkken [27] investigated the dynamic stiffness of caisson foundations for subsea structures and the effect of added soil mass on the earthquake response of these structures. Kaynia [1] presented a comprehensive study on the dynamic response of 4-pile, caisson and mudmat foundations for subsea facilities and the effect of soil-structure interaction and radiation damping on the seismic performance of these foundations.

Some studies have addressed the liquefaction response of offshore foundations and anchors in recent years using advanced numerical modeling ([32–39]). Kazemi Esfeh and Kaynia [38] focused on establishing a reliable three-dimensional numerical model for liquefaction response of anchor piles under a combination of static mooring load and earthquake shaking. In this study, calibrated soil parameters were confirmed using element-level and centrifuge tests, and different model features including boundary conditions, mesh size, and large-strain were investigated. Subsequently, they extended their research to the earthquake response of monopiles and caissons with various dimensions for large offshore wind turbines subjected to a combination of wind load and earthquake shaking [39]. This research showed that foundations for offshore wind turbines in deep liquefiable soil could experience considerable rotations even during moderate ground shakings due to the unsymmetrical loading caused by wind.

The present study investigates the earthquake response of caisson and mudmat foundations supporting subsea manifolds in liquefiable sand subjected to moderate and strong ground motions. To this end, three-dimensional, non-linear dynamic analyses were carried out for a total of eleven cases using advanced numerical modeling. The analysis cases include six computational models representing manifolds with different weights and sizes supported by caissons and mudmats in shallow and deep liquefiable sand subjected to four earthquake loading conditions. Moreover, the post-liquefaction responses of the caisson and mudmat in two of the cases were evaluated by performing coupled fluid flow analyses. The results are presented in terms of excess pore water pressure and shear stress-strain response in the soil together with earthquake-induced displacements of the foundation. In all these cases, the structure was placed symmetrically on the foundation which minimized the tilt due to earthquake shaking.

1.1. Structural models and earthquake loading

The three-dimensional analyses were performed using the commercial finite difference program FLAC3D. The fluid-flow scheme was used in conjunction with the dynamic analyses to simulate the time-dependent variations in the pore water pressure during liquefaction and the dissipation of excess pore pressure after liquefaction. The formulation of fluid-mechanical analysis in FLAC3D is based on the coupled formulations of poromechanics originated by Biot [40]. Modeling details are presented in the following sections.

For the earthquake analyses, the two earthquake records Kobe-L and Northridge-Newhall were used after baseline-correction and filtering. The acceleration time histories and corresponding 5% acceleration response spectra for these events are shown in Fig. 2a and Fig. 2b, respectively. These ground motions represent extreme loading conditions that could only occur in areas of high seismicity. To

Table 1
Numerical models considered in the present study.

Model name	Foundation type	Caisson diameter, D/ Mudmat side, B [m]	Skirt length, h [m]	Manifold mass, m [t]	Manifold dimensions (B × L × H) [m]	Thickness of liquefiable soil layer [m]	Loading[a]
C80	Caisson	5	8	80	15 × 15 × 5	19	KL, KLr, N–N, KL-V
C150	Caisson	8	12	150	15 × 15 × 5	19	KL
M80	Mudmat	15	–	80	15 × 15 × 5	19	KL
M150	Mudmat	15	–	150	15 × 15 × 5	19	KL, KLr, N–N
C80H	Caisson	5	8	80	7 × 15 × 15	19	KL
M150S	Mudmat	15	–	150	15 × 15 × 5	5	KL

[a] KL = Kobe-L, KLr = Kobe-L reduced to 30%; N–N= Northridge-Newhall, KL-V=Combined Kobe-L and Kobe-UP.

evaluate the response of subsea foundations in liquefiable sand due to less severe earthquake shakings, representing moderate seismicity, the responses of two of the subsea foundation cases were also computed by reducing the Kobe-L earthquake shaking by 70%. Table 1 presents the earthquake shaking applied to the base of each model. Besides, for one of the models described in the following, the effect of simultaneous action of horizontal and vertical shaking on the excess pore pressures and the response of the structure was studied. Fig. 2c shows the acceleration time history for the vertical component of the Kobe earthquake used in the bi-directional shaking analysis.

1.2. Geometry and boundary conditions

Fig. 3 illustrates the three-dimensional models and mesh used for the cases with mudmat foundation (Fig. 3a) and with caissons (Fig. 3b). Quadrilateral elements were used to model the soil, foundation and manifold. The mesh size was determined in a way to allow at least 10 elements for wavelength corresponding to elastic shear modulus at each depth and frequency content of the input motion. Due to symmetry, only half of the model was studied and boundary conditions were accordingly applied to the plane of symmetry. A sensitivity analysis was carried out to determine the optimum size of the model for a satisfactory balance between accuracy and computational effort. The soil model was 60 m long, 18 m deep, 26 m high and consisted of 19 m of loose Ottawa sand F65 with a void ratio $e = 0.7$ and saturated unit weight $\gamma_{sat} = 19.1$ kN/m^3 overlying 7 m of dense Ottawa sand F65 with $e = 0.56$, $\gamma_{sat} = 19.9$ kN/m^3 (Fig. 3). In one of the models in this study, the thickness of the loose Ottawa sand layer was reduced to 5 m to investigate the effect of the thickness of liquefiable soil layer on the response of the foundation (Table 1).

For the lateral boundary conditions, the tied boundary condition was employed since it has been shown to provide the most stable and accurate results compared to the conventional viscous boundary conditions using horizontal and vertical dashpots on the boundary in combination with the imposition of free-field motions [39]. The better performance of the tied boundary is demonstrated in Fig. 4 which compares the simulated and measured excess pore pressure values at several depths in the centrifuge as reported in Ref. [41]. The comparison clearly verifies the superior performance of the tied boundary for the present application. These results also indirectly confirm the adequacy of the selected mesh size for these analyses.

The manifold was modeled as a solid square box with side B and height H (Fig. 3c). In one of the models considered in this study, the manifold was placed by rotating it 90° to investigate the effect of geometry variations (Table 1). The masses given to the various manifold models include both the structural mass of the manifold and the hydrodynamic added mass related to the vibration of the structure in water. The hydrodynamic load on a vibrating submerged body requires special analyses which become very demanding in the case of a real manifold consisting of a complex assembly of various elements such as pipes and plates. Therefore, in most engineering applications, the hydrodynamic effects are replaced by approximate hydrodynamic added mass to the structure's mass. This approach was adopted in this research as it is considered sufficient for the objectives of the study.

The caisson was modeled as an open-ended cylinder with a skirt-length to diameter ratio of h/D = 1.5 and a skirt wall thickness of 0.04 m, as typical dimensions used for caissons supporting subsea structures in practice [1]. A gap of 0.5 m was considered between the manifold and the seabed to ensure that the manifold is not in direct contact with the ground, as typical of subsea structures installed on caissons (e.g. Ref. [13]). Even in cases when the base of the structure comes in touch with the seabed during installation, there is not a full contact between the structure and the soil and the partial contact is gradually lost over time due to erosion or soil settlement under the base.

The mudmats were considered as square plates of side B with the same base dimensions of the manifold; thus, the mudmats were not modeled independently. In other words, manifolds and mudmats were considered as a single unit (see Fig. 1). Moreover, as described earlier, skirts are often very short and primarily meant for easier installation and also for ensuring better bond with the soil. They sometimes provide protection against erosion around the foundation. These skirts do not add any appreciable lateral resistance during liquefaction, especially considering the low soil strength close to the seabed, nor do they have any noticeable effect on the dynamic response of the foundation. Therefore, they are not explicitly modeled as they require special treatments with respect to mesh size and stress concentration in the soil at their edges.

This study includes six models of caissons and mudmats featuring different dimensions supporting manifolds with various sizes and weights in shallow and deep liquefiable sand, as listed in Table 1. These models are representatives of subsea foundations and manifolds used in the industry [1] and are chosen to assess the performance of subsea foundations in liquefiable soil during and after

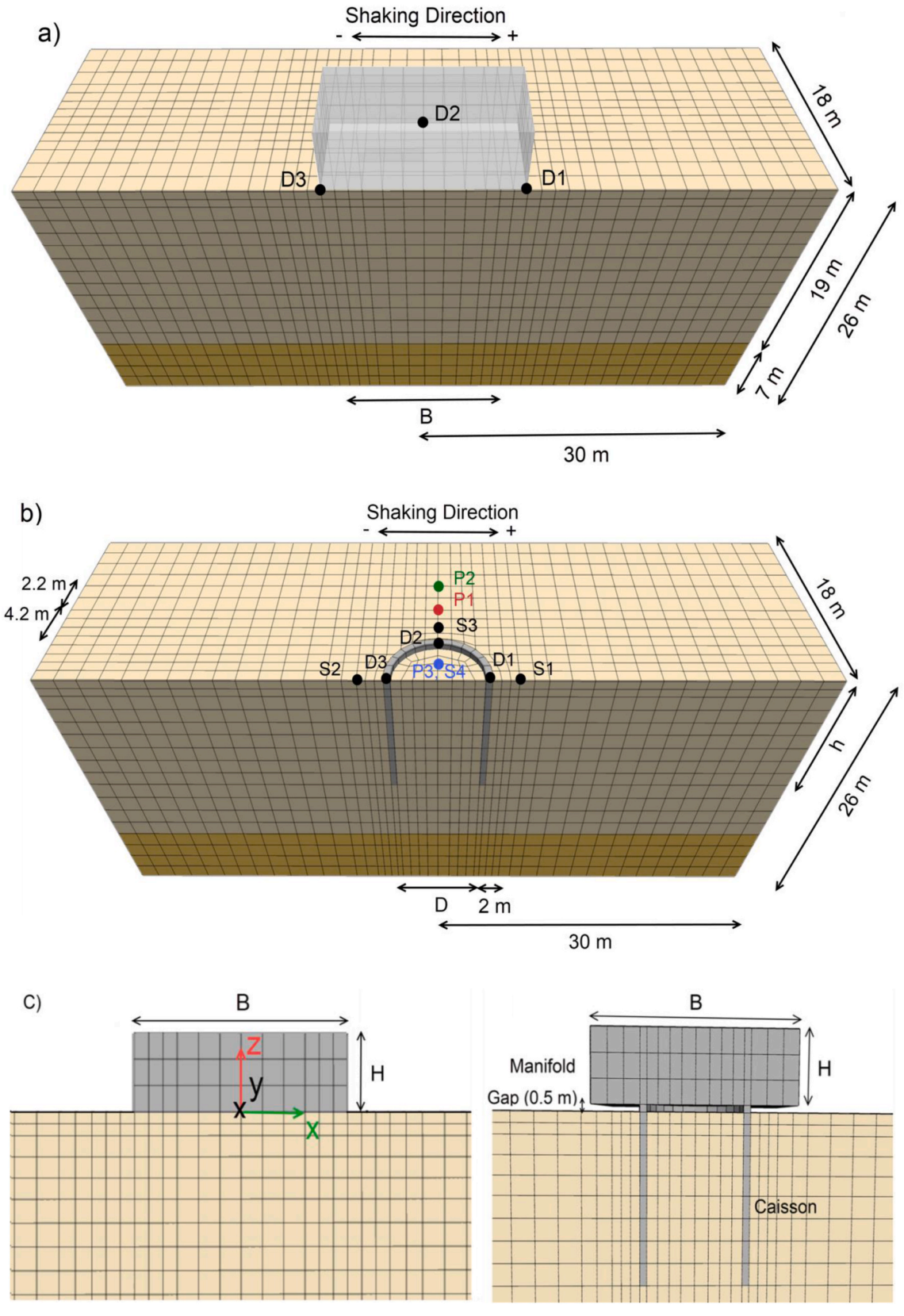

(caption on next page)

Fig. 3. Finite difference meshes of a) mudmat, b) caisson and c) manifold models together with monitoring points for computing excess pore pressure and stress-strain response in the soil along with displacements of the foundation.

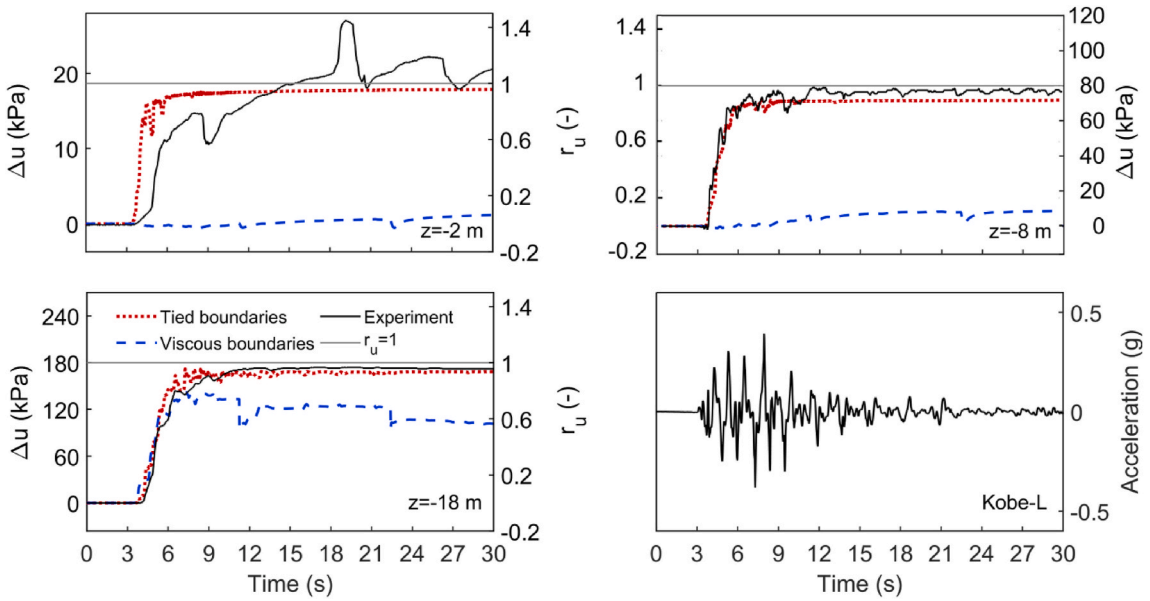

Fig. 4. Comparison of experimental and numerical excess pore pressures using different boundary conditions.

Table 2
SANISAND constitutive model parameters calibrated for Ottawa sand F65 [25].

Parameter	value
Nondimensional elastic modulus factor, G_0	125
Poisson's ratio, υ	0.05
Critical state stress ratio, M	1.26
Ratio of critical-state stress ratio in extension and compression, c	0.735
State line constant, λ_c	0.0287
Void ratio at p = 0, e_0	0.78
State line constant, ξ	0.7
Yield surface constant, m	0.02
h_0	5
c_h	0.968
n^b	0.6

ground shaking.

In principle, structures with the same weight but different geometries could have different earthquake responses because geometry variations lead to changes in the natural frequency and loading on the foundations. Since manifolds vary in shape and size, their performance might be different during liquefaction. Thus, model C80H was developed to investigate the effect of geometry variations on the dynamic response of the structure. All features and parameters of model C80H are the same as in model C80 while a larger height was considered for the manifold in this model (see, Table 1).

1.3. Material and interface properties

The SANISAND constitutive model was employed to simulate the behavior of the saturated Ottawa sand. SANISAND is the name of a family of simple anisotropic sand constitutive models developed within the framework of critical state and bounding surface plasticity. Over the past few decades, the model has been extended to capture additional features of sand's behavior under different loading conditions. In the present study, a version of the SANISAND model accounting for the effect of fabric change developed by Dafalias and Manzari [42] was used. The soil parameters are listed in Table 2. These parameters were calibrated by Ramirez et al. [43] using FLAC and validated by Kazemi Esfeh and Kaynia [38,39] for three-dimensional analyses in FLAC3D. The bulk modulus and density of water were taken as 2 GPa and 1000 kg/m^3. A Rayleigh damping with damping ratio $\xi = 3\%$ at the first and third natural frequencies of the soil deposit ($f_{n,1} = 1.72$ Hz and $f_{n,3} = 8.61$ Hz) was used in the dynamic simulations.

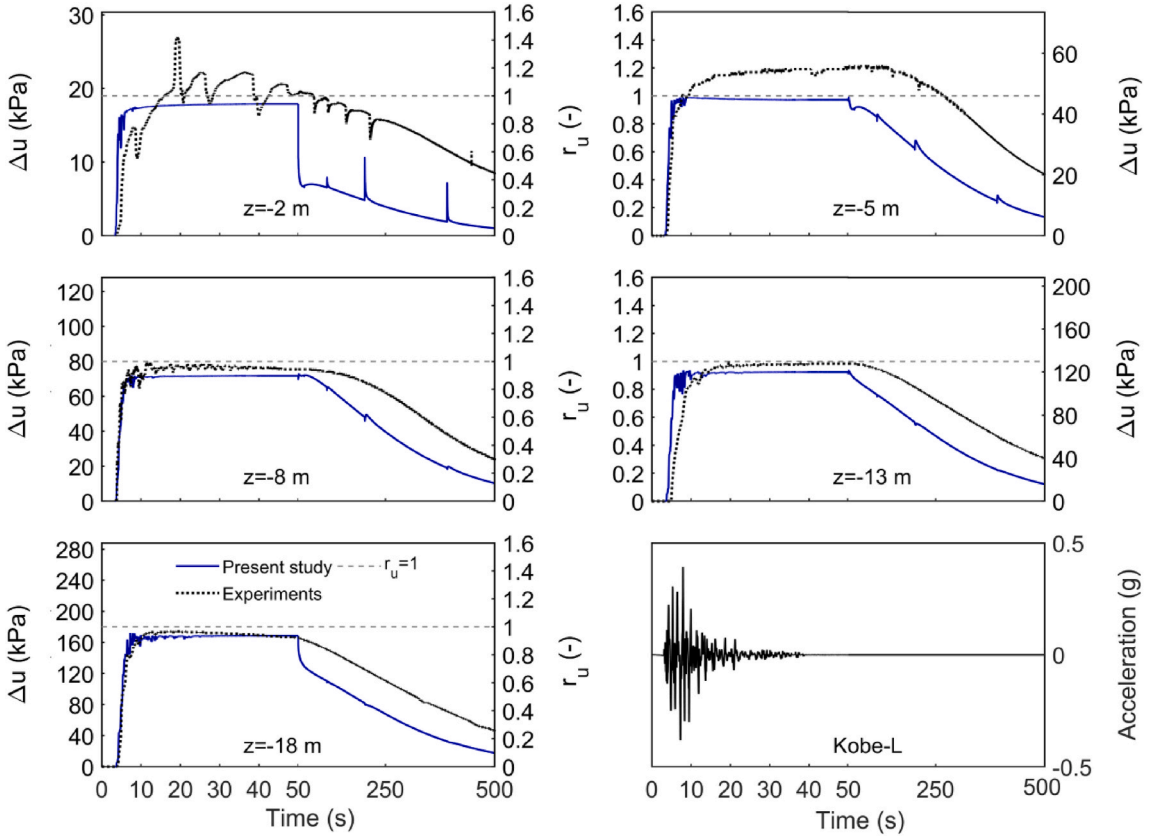

Fig. 5. Comparison of numerical and experimental excess pore water pressure time histories for simulations of site response in the centrifuge test during and after the shaking.

The linear elastic model with Young's modulus $E_{steel} = 210$ GPa and density $\rho_{steel} = 8000$ kg/m^3 was assigned to the steel structures (i.e. foundation and manifold). To avoid large aspect ratios of elements in the caisson models, which may result in numerical instabilities or large computational time, the wall thickness of the skirt was increased from 0.04 m to 0.5 m, and the elastic modulus and mass density of the skirt were accordingly reduced. The equivalent elastic modulus E_{eq} and mass density ρ_{eq} were determined in a way that the bending rigidity and total mass of the equivalent skirt are equal to those of the real foundation. This simplification does not have any impact on the response of the soil nor the foundation, especially because the foundation behaves almost rigidly. This procedure was used for anchor piles in Ref. [38] where more details are provided. Following this scheme, an equivalent elastic modulus $E_{eq} = 17.54$ GPa, and a unit mass $\rho_{eq} = 2450$ kg/m^3 were computed for the skirt in model C150, and similarly, an equivalent elastic modulus $E_{eq} = 21.26$ GPa, and unit mass $\rho_{eq} = 2480$ kg/m^3 were calculated for the caisson skirts in models C80 and C80H.

For the caisson models, soil-structure interfaces were created on the zone faces around the skirt. An elastic-perfectly plastic constitutive law obeying the Mohr-Coulomb criterion was considered. The interface friction angle was taken as 2/3 of the internal friction angle of loose Ottawa sand (i.e. $\varphi_p \sim 32^\circ$, see Ref. [38]) and normal and shear stiffnesses of the interface were set to ten times the stiffness of adjacent zones.

For mudmat foundations, the analyses refer to a solid base plate, considering that the skirts ensure a fully bonded interface in undrained conditions, consistent with previous studies ([9,10]).

2. Numerical simulation

The six models described in Section 2.1 were subjected to four different moderate and strong mono-directional and bi-directional earthquake shakings leading to a total of eleven analysis cases, as presented in Table 1.

The performance of the computational model and modeling features were validated in Refs. [38,39] using the results of a centrifuge test with free-field conditions (i.e. with no structure) [41]. Since the results of a centrifuge test of the dynamic response of subsea foundations in liquefiable sand are not available, as comprehensively discussed in Section 1, the computed responses in the present study could not be compared with experimental results. Therefore, while the trends of the results presented in the present study are believed to be qualitatively correct, it is advised that the numerical values be used mainly in a comparative sense.

In the following, details of numerical simulations, loading conditions and model validations are presented.

2.1. Computational steps

In the numerical computations, first, the fluid flow was turned on to establish the initial pore pressure in the soil domain. Afterward, the fluid flow was switched off during the shaking such that the pore pressure generation was only due to the volume change in the soil matrix (i.e. no drainage), meaning that the response was undrained. During an earthquake with a shaking of the order of 20 s, with many high frequency cycles, the drainage is practically zero except for a small layer close to the mudline. The use of effective stress analyses combined with the undrained condition has in fact become a standard solution for earthquake response in sand and this is also the procedure conventionally adopted in design. This is also applicable to the sands considered in this study whose permeability was measured in the order of 10^{-4} m/s.

In two of the analysis cases in this research, the post-liquefaction settlement of the foundation and the rate of dissipation of excess pore pressure were assessed by carrying out coupled fluid-mechanical analyses after the dynamic simulations. In these analyses, the flow was allowed at the seabed surface while all other boundaries of the model were considered impermeable.

In all the simulations, caissons and manifolds were considered impermeable; thus, the null fluid constitutive model and zero porosity were assigned to their zones. In a sensitivity analysis carried out in Ref. [38], the results of dynamic simulations in both small-strain and large-strain modes were compared. These results were found to be very similar indicating that the small-strain assumption is satisfactory for the range of responses considered in this paper. Moreover, the small-strain models are less prone to numerical instabilities. Therefore, the dynamic analyses were performed using the small-strain solution to reduce the computational time.

2.2. Validation of constitutive model

Kazemi Esfeh and Kaynia [38,39] have recently validated the soil parameters calibrated by Ramirez et al. [43] for three-dimensional analyses in FLAC3D and confirmed that the SANISAND constitutive model is capable of reproducing the three-dimensional site response of a liquefiable soil deposit in a centrifuge test [41]. A layered sand deposit composed of Ottawa sand F65 and Monterey sand with a height of 18 m, was subjected to the Kobe-L earthquake record (Fig. 2a) and the site response was computed at different depths of the soil profile (z = −18, −13, −8, −5, −2 m) during the shaking. The soil parameters presented in Table 2 were used for the Ottawa sand. The details of these model validations can be found in Refs. [38,39].

Fig. 5 displays a comparison between the numerical and experimental excess pore pressures, Δu, together with the corresponding excess pore pressure ratios ($r_u = \Delta u/\sigma'_{v0}$, where σ'_{v0} is the initial effective vertical stress) at different depths in the soil profile. The limit $r_u > 0.95$ was regarded as liquefaction criterion. As shown in Fig. 5, the model is capable of consistently predicting the measured pore pressure buildup during the shaking while the dissipation rate is overestimated. This intrinsic shortcoming of SANISAND model is also reported by other researchers [43]. A good agreement can be observed between the dissipation responses computed in the present study and those presented by Ramirez et al. [43] confirming the consistent performance of the computational model developed used in this study. Furthermore, a good agreement is observed between the numerically computed and analytically estimated consolidation settlements at the surface of the free-field model. Thus, the results of the presented study are believed to be qualitatively correct; however, numerical values should primarily be used in a comparative sense.

2.3. Evaluation of numerical simulations

To assess the soil response as liquefaction develops during the shaking, the excess pore pressures at monitoring points P1–P3 were computed. The initial effective overburden stresses at monitoring points before the earthquake shaking were considered as the sum of the in-situ and additional effective vertical stresses due to the weight of the structure to be used in calculations of the excess pore pressure ratios at each depth.

Since the soil inside the caisson is under greater confining pressure, large excess pore pressures can be generated in the inner soil during the strong shaking. Nevertheless, a different mechanism, namely kinematic confinement of the soil due to large stiffness of the caisson, which can reduce/inhibit strains in the soil inside the caisson, is expected to result in overall lower excess pore pressures. Therefore, monitoring point P3 was chosen for the caisson models to investigate the potential reduction in pore pressure ratios inside the caisson.

Additionally, the shear stress-strain responses at monitoring points S1–S4 in the caisson models were computed to evaluate the accumulation of strain inside and outside the caisson as liquefaction develops. To assess the permanent and transient displacements and rotation of the foundation during the shaking, the horizontal and vertical displacements were monitored at points D1-D3 on top of the caisson and at the corners of the manifold, in the case of mudmats.

3. Results and discussions

The performances of the manifolds on caissons and mudmats during the earthquake shaking were assessed by monitoring the excess pore water pressure and shear stress-strain responses in the soil around the foundations together with the earthquake-induced transient and permanent displacements of the foundations.

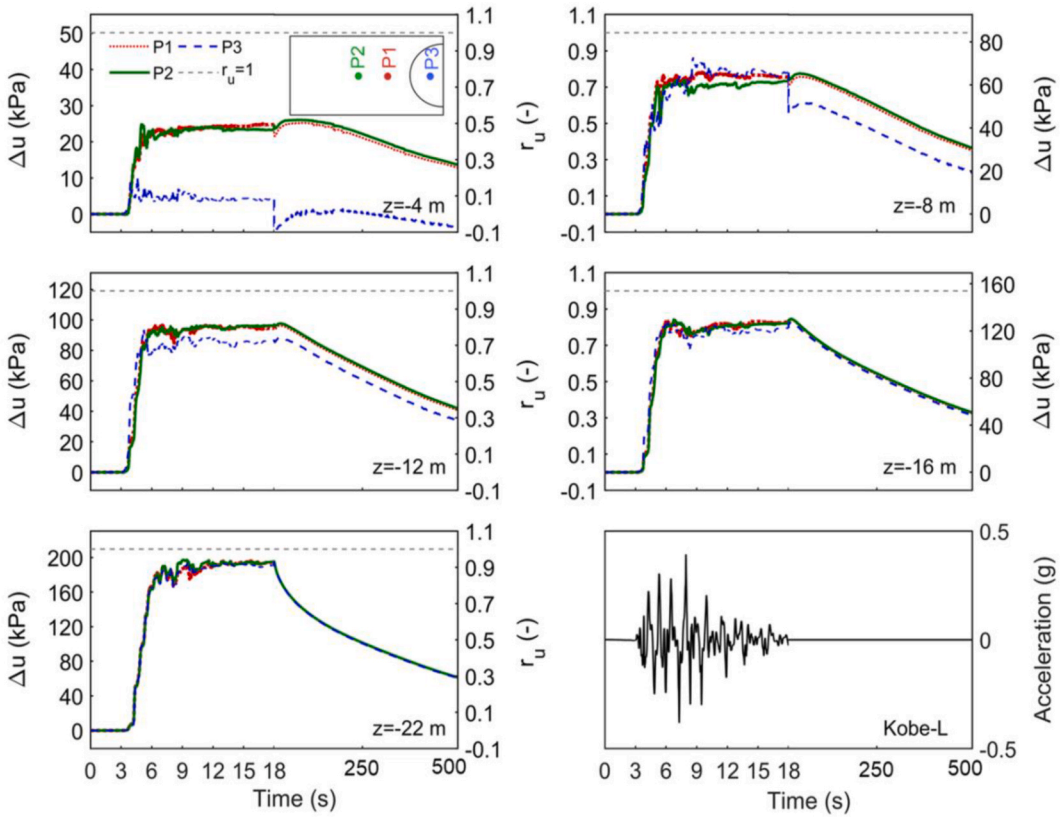

Fig. 6. Time histories of excess pore pressure at monitoring points in model C80 during and after Kobe-L earthquake shaking.

3.1. *Response of foundations for different loading conditions*

Fig. 6 displays the time histories of simulated excess pore water pressures at monitoring points at various depths for model C80 subjected to Kobe-L earthquake shaking. As shown in the figure, excess pore pressure ratios at all points and depths tend to one. Moreover, it can be observed that the excess pore pressure is lower inside the caisson (point P3 at depth $z = -4$ m) which is believed to be due to the kinematic confinement provided by the caisson described above. This feature can be observed more clearly in Fig. 7b that illustrates the pore pressure contour at the end of the Kobe-L earthquake shaking for model C80 with a refined mesh. Sensitivity analyses for mesh size indicated that the distribution and values of pore water pressure do not change remarkably by further refining the computational mesh. Nonetheless, for a better illustration of variations in pore water pressure around the caisson, the pore pressure contour corresponding to analyses with the refined mesh shown in Fig. 7a is presented.

Fig. 8 compares the computed acceleration time histories together with their response spectra on top of the manifolds in models C80 and M80. A larger amplification is observed in C80, which is attributed to the larger effect of soil-structure interaction (SSI) in the case of caisson foundation. The mudmat has larger contact with the soil and a larger rocking stiffness resulting in less rotation of the foundation which is directly related to the horizontal acceleration on top of the mudmat.

Fig. 9 presents the time histories of the simulated horizontal, vertical and rotational displacements of the caisson in model C80 subjected to Kobe-L acceleration input. A downward sinking of about 18 cm was computed during the shaking, with the caisson experiencing a small permanent rotation of 0.1 deg and a horizontal displacement of 3 cm in the direction of shaking at the end of earthquake loading. The rather small permanent horizontal displacement and rotation are, as expected, due to the generally symmetric earthquake motions and symmetrical structure. After the shaking, the caisson undergoes further settlements of about 4 cm due to post-liquefaction dissipation of excess pore pressure while, as expected, no change in horizontal displacement or rotation of the caisson can be observed during this process. Fig. 10 illustrates the exaggerated deformed mesh of the caisson model C80 and displacement vectors at the end of the Kobe-L ground shaking that clearly demonstrate the sinking of the caisson due to liquefaction.

Figs. 11 and 12 display time histories of the shear strains and shear stresses at monitoring points at depths 4 m and 8 m in model C80 subjected to the Kobe-L earthquake shaking. These results reveal that both shear strains and stresses at monitoring points reach their peaks during the strong shaking and subsequently diminish as the soil reaches the full liquefaction state. Considerably lower shear strain accumulation can be observed inside the caisson (point S4 at $z = -4$ m) than outside that confirms the effect of kinematic confinement, as discussed earlier.

Fig. 13 presents the time histories of the simulated excess pore water pressures at monitoring points for the model C80 subjected to

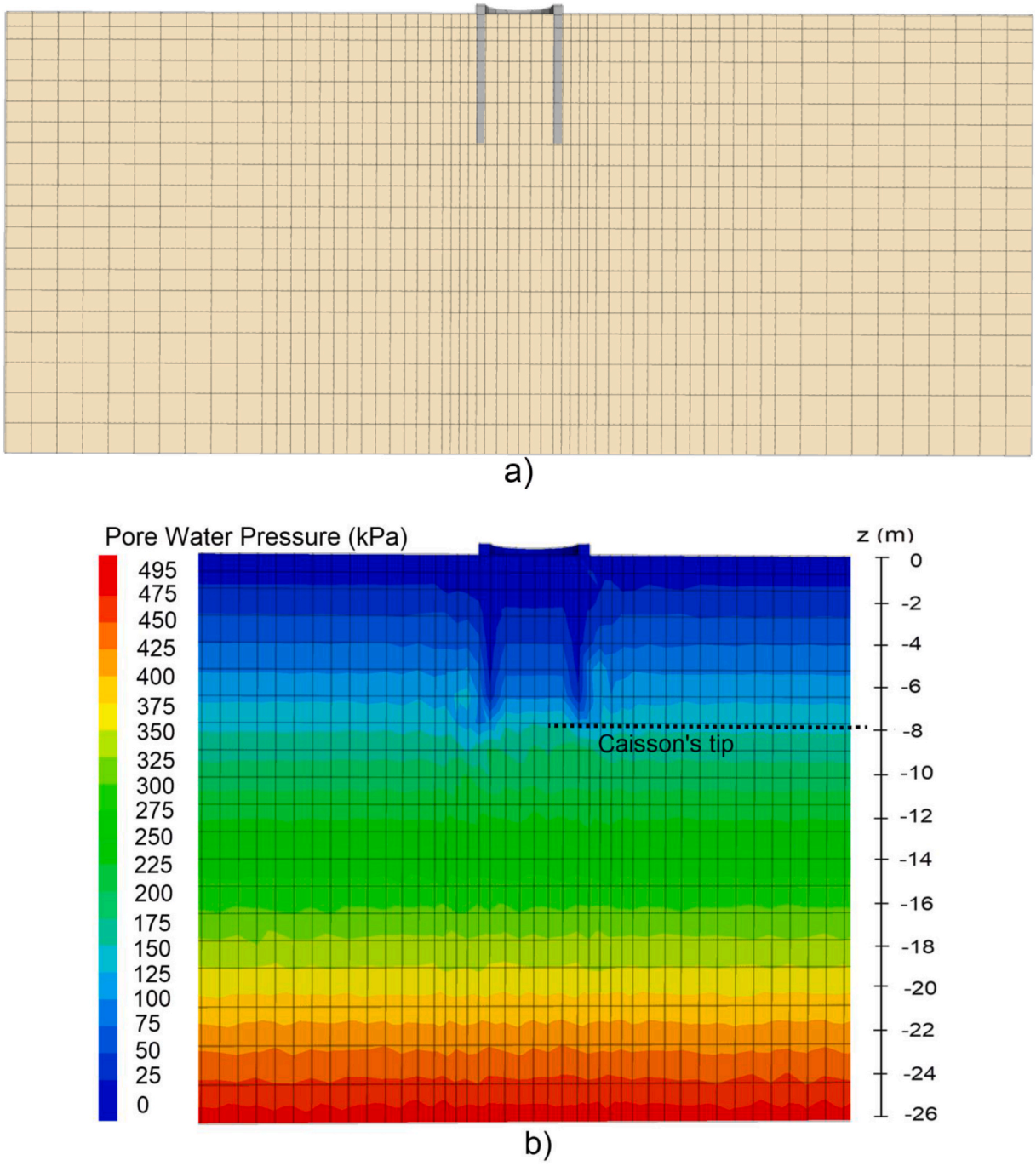

Fig. 7. a) Refined computational mesh and b) contours of pore water pressure close to the caisson at end of Kobe-L earthquake shaking in model C80.

Northridge-Newhall ground shaking. The response patterns of excess pore pressure and the final values of excess pore pressure ratio at monitoring points are similar to those for the caisson model C80 under the Kobe-L ground motion.

Fig. 14 displays the computed acceleration time history and its response spectrum at the top of the manifold in model C80 subjected to Northridge-Newhall ground motion. A de-amplification of acceleration can be observed, indicating the low spectral acceleration of Northridge-Newhall earthquake shaking at the natural frequency of the caisson-soil-manifold system that is about 1.1 s.

Fig. 15 presents the horizontal, vertical and rotational displacements of the caisson in model C80 subjected to Northridge-Newhall ground motion. The plots in the figure indicate that the caisson experiences a larger horizontal displacement of about 7 cm, under this earthquake compared to the case it is subjected to Kobe-L earthquake shaking (Fig. 9). However, almost the same vertical displacement

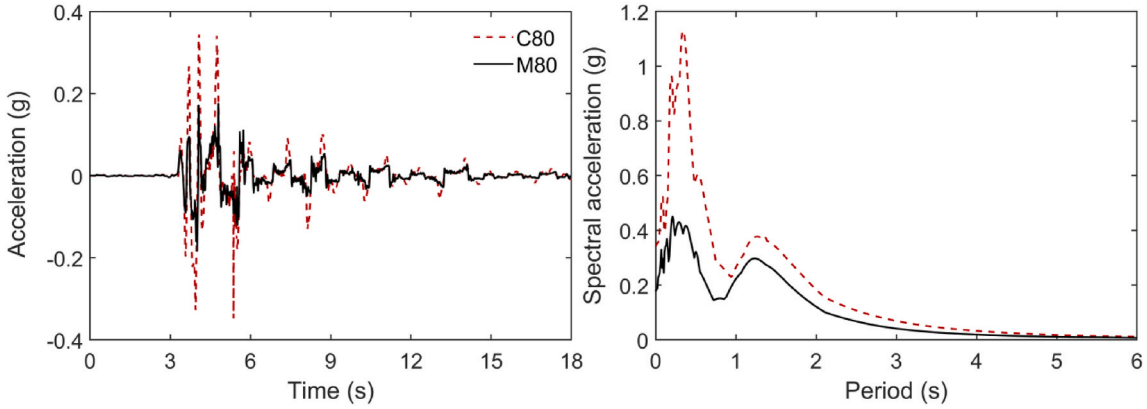

Fig. 8. Comparison of acceleration time histories and spectra at top of manifold on caisson in model C80 and mudmat in model M80 subjected to Kobe-L earthquake shaking.

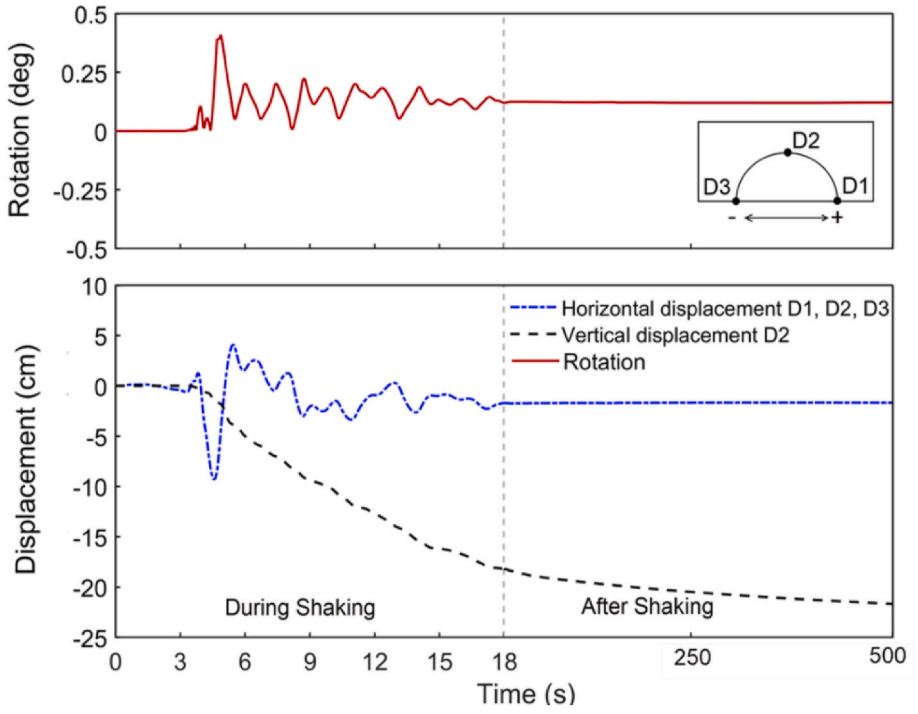

Fig. 9. Time histories of horizontal, vertical and rotational displacements of caisson in model C80 during and after Kobe-L earthquake shaking.

and rotation of the caisson are estimated for both earthquake shaking. The larger sliding displacements can be attributed to the specific characteristics (including higher Peak Ground Acceleration, PGA) of Northridge-Newhall ground motion (see, Fig. 2b).

Fig. 16 shows the simulated excess pore water pressures in the soil for the Kobe-L earthquake shaking reduced by 70%. The results indicate that the sand still liquefies at most of the points even under the reduced shaking, however, it takes longer for these points to reach the full liquefaction state.

Table 3 lists earthquake-induced displacements of subsea foundations at the end of earthquakes in different cases. In general, subsea foundations experience considerable sinking movements during liquefaction while only small rotations can be observed during the shaking. Nonetheless, the results indicate that manifolds on caissons could potentially undergo larger settlements during liquefaction. For example, the manifold on caisson in model C80 experiences a downward sinking movement of 18 cm at the end of Kobe-L earthquake whereas, a vertical displacement of only 9 cm can be observed for the same manifold on mudmat in model M80 under the same earthquake shaking (see, Table 3). The same comparison is valid for vertical displacements of manifolds in models C150 and M150. Although the caisson in C80 and the mudmat in M80 experience different levels of vertical displacements during the shaking, the consolidation analyses indicated that post-liquefaction settlements of 4–5 cm could occur in both foundations. Fig. 17 shows an

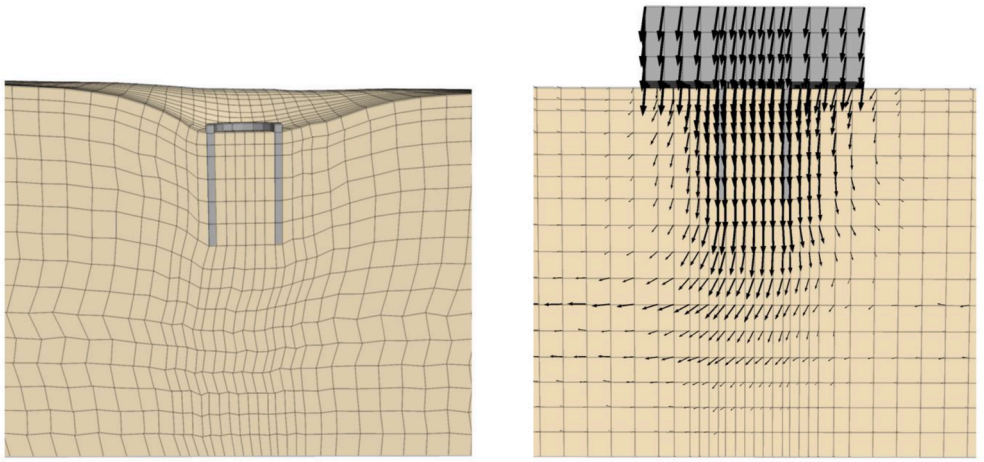

Fig. 10. Deformed mesh (exaggerated for illustrative purposes) and displacement vectors at the end of Kobe-L earthquake shaking in model C80.

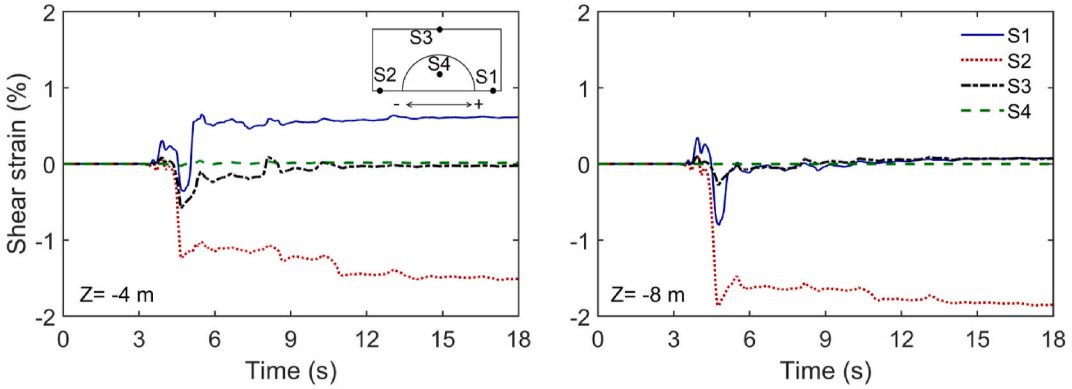

Fig. 11. Time histories of shear strain at monitoring points at depths z = −4 m and z = −8 m in model C80 subjected to Kobe-L earthquake shaking load.

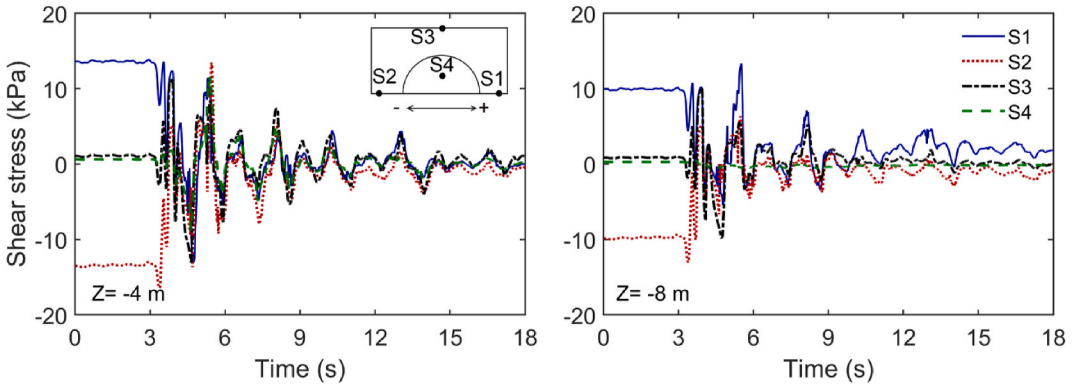

Fig. 12. Time histories of shear stress at monitoring points at depths z = −4 m and z = −8 m in model C80 subjected to Kobe-L earthquake shaking load.

exaggerated deformed mesh of the soil in model M150 at the end of the Kobe-L earthquake that more clearly demonstrates the downward movements of the structure. The main reason for less settlement of mudmats could be that, in general, they are lighter than caissons. Moreover, mudmats are in contact with a large area on the seabed (that is, the gravitational load of the manifold is distributed over a large area of soil).

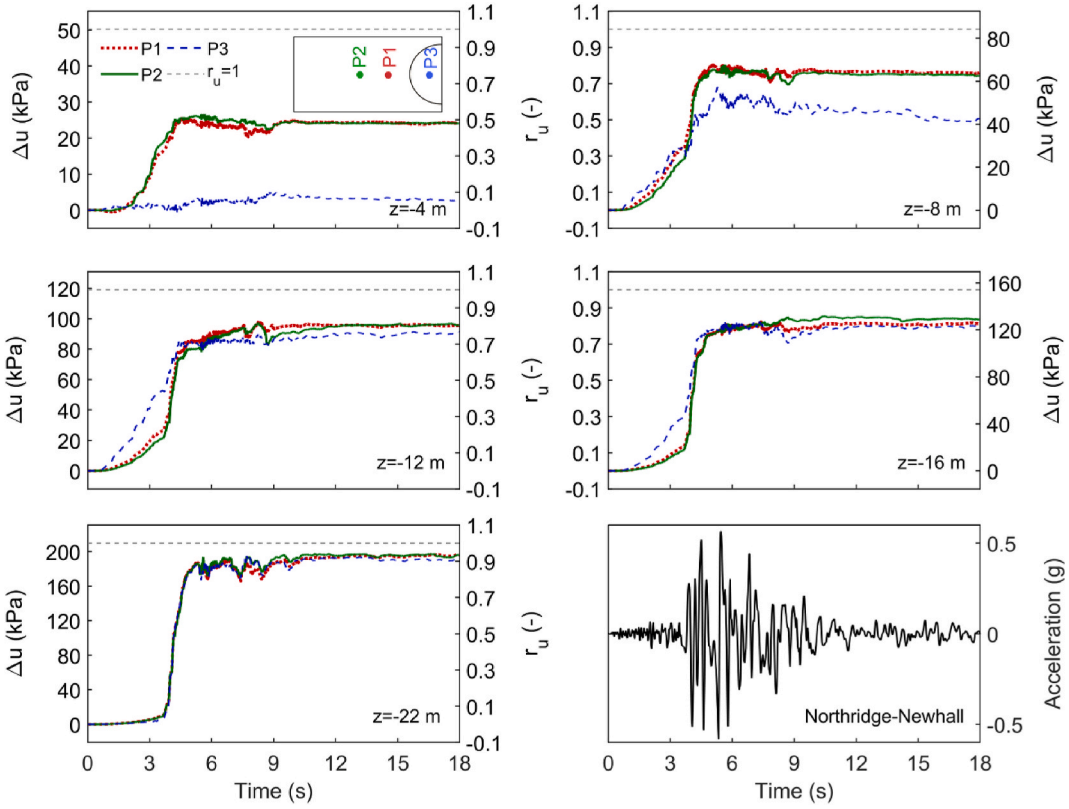

Fig. 13. Time histories of excess pore water pressure at monitoring points in model C80 subjected to Northridge-Newhall earthquake shaking.

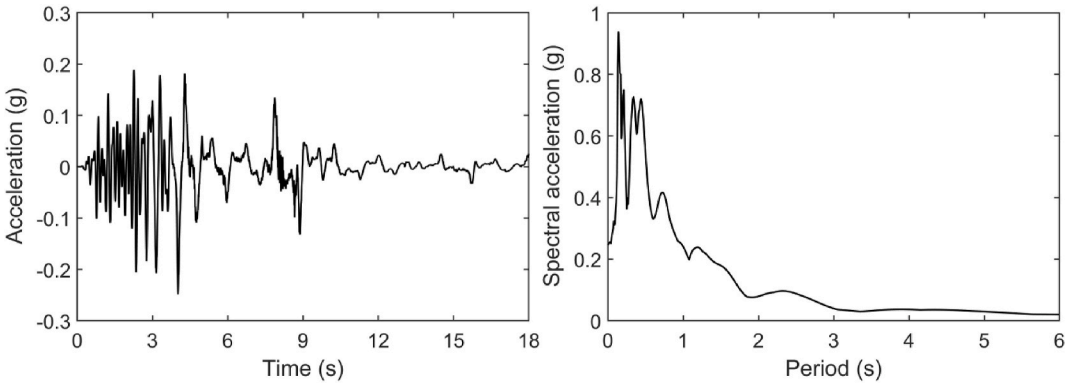

Fig. 14. Acceleration response at top of manifold in model C80 subjected to Northridge-Newhall earthquake shaking.

A comparison between the horizontal, vertical and rotational displacements of the caissons in models C80 and C150 (see, Table 3) indicates that the larger diameter of caisson model C150 (with almost the same length to diameter ratio as in model C80, L/D ~ 1.5) has led to lower earthquake-induced displacements and rotation in this case even though the manifold is almost twice heavier in model C150 (that is, 150 tones compared to 80 tones in model C80).

Both caisson and mudmat foundations in models C80 and M150, experience larger horizontal displacements under the Northridge-Newhall earthquake shaking which is believed to be due to the higher PGA of Northridge-Newhall earthquake compared to that of Kobe-L motion (see, Fig. 2b). As an example, the permanent horizontal displacement of 9 cm in the direction of shaking is computed in model M150 when the structure is subjected to Northridge-Newhall ground shaking whereas, it experiences a sliding displacement of 4 cm under the Kobe-L earthquake shaking.

As expected, subsea foundations in models C80 and M150 experience less settlement under the Kobe-L earthquake shaking when reduced to 30% (see, Table 3). For instance, the permanent vertical displacement of the caisson in model C80 is 23% lower under the

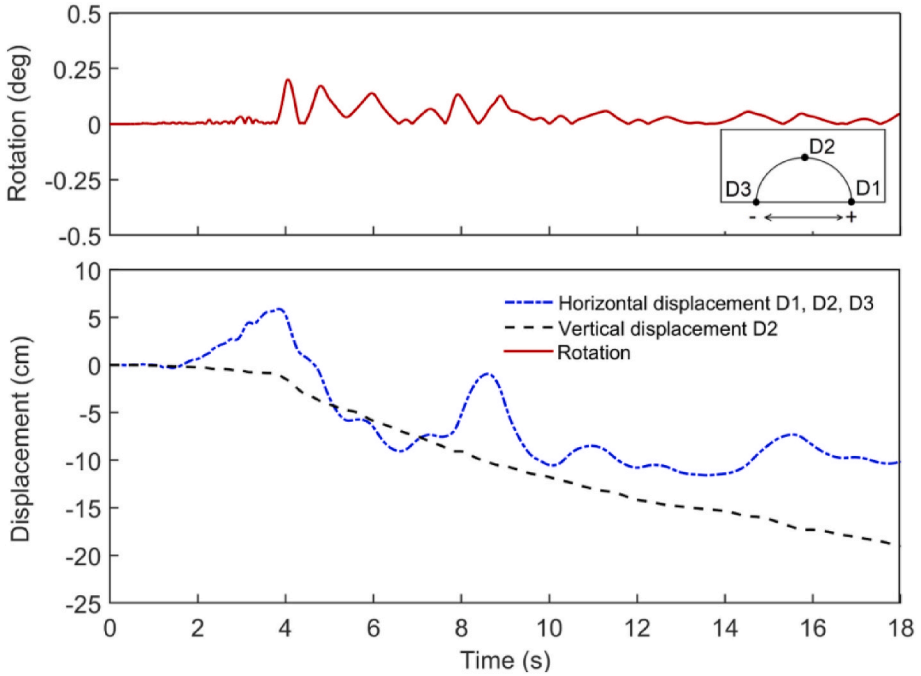

Fig. 15. Time histories of horizontal, vertical and rotational displacements of caisson in model C80 subjected to Northridge-Newhall earthquake shaking.

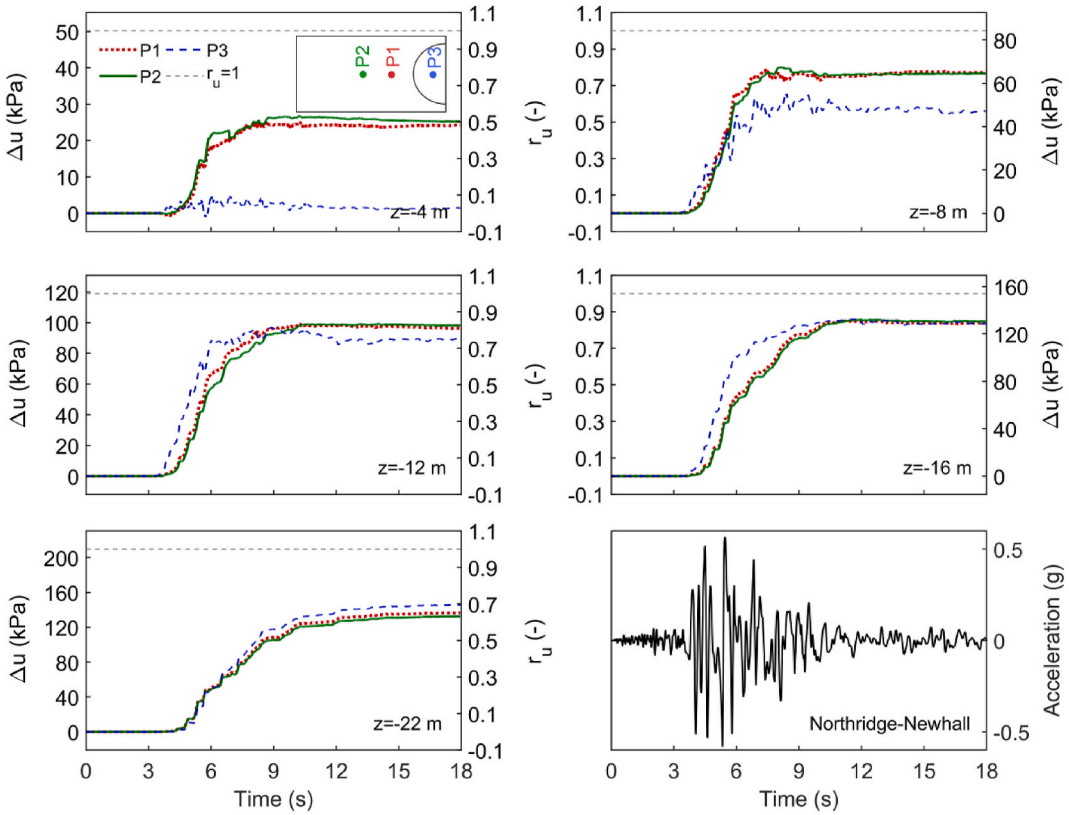

Fig. 16. Time histories of excess pore water pressure at monitoring points in model C80 subjected to Kobe-L earthquake shaking reduced by 70%.

Table 3
Computed earthquake-induced displacements of subsea foundations at the end of the earthquake in different cases.

Model name/Earthquake loading	Horizontal displacement (cm)	Vertical displacement (cm)	Rotational displacement (deg)
C80/Kobe-L	−3	−18	0.10
C150/Kobe-L	0	−16	0.08
M80/Kobe-L	−5	−9	0
M150/Kobe-L	−4	−12	0
C80H/Kobe-L	−1	−20	0
C80/Kobe-L reduced to 30%	−4	−14	0.05
M150/Kobe-L reduced to 30%	−3	−8	0
C80/Northridge-Newhall	−10	−19	0
M150/Northridge-Newhall	−9	−11	0

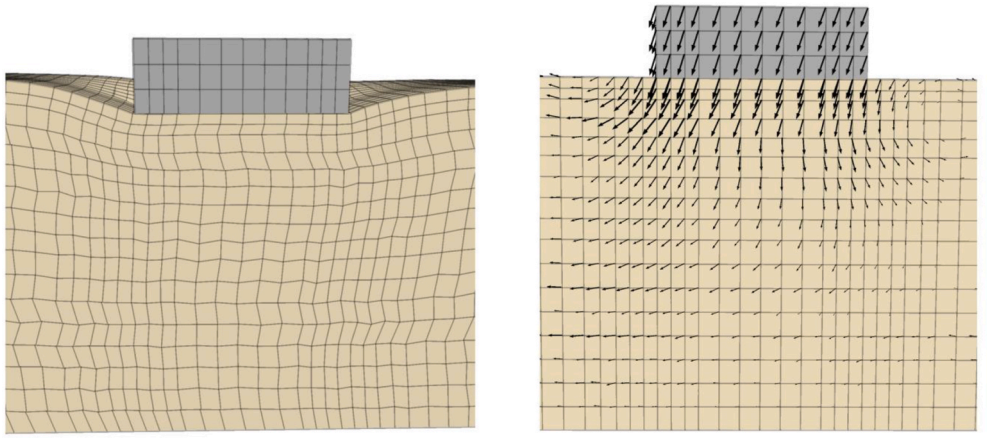

Fig. 17. Deformed mesh (exaggerated for illustrative purposes) and displacement vectors at the end of Kobe-L earthquake shaking in model M150.

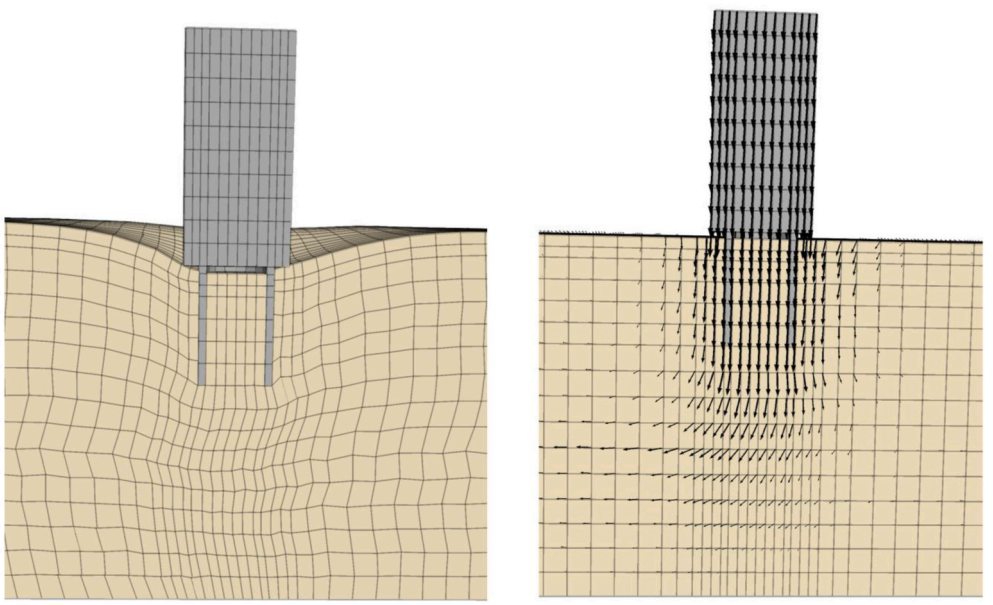

Fig. 18. Deformed mesh (exaggerated for illustrative purposes) and displacement vectors at the end of Kobe-L earthquake shaking in model C80H.

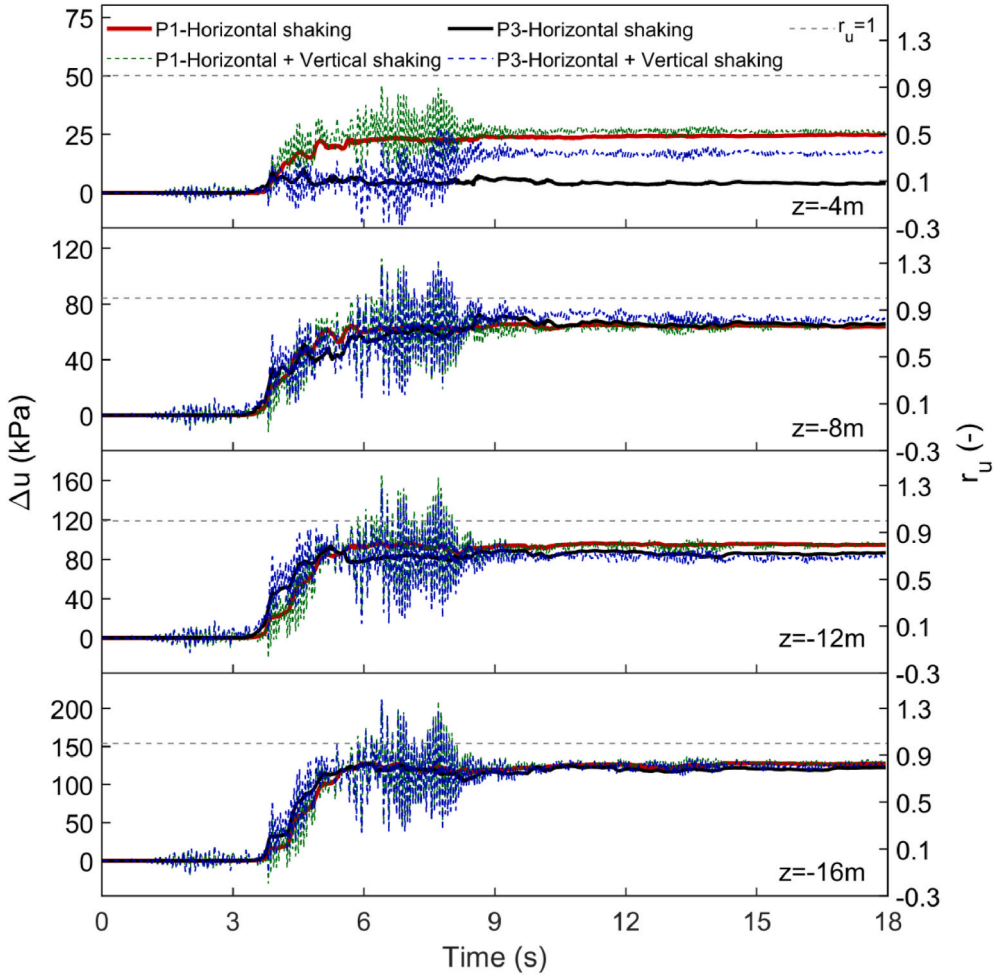

Fig. 19. Comparison of excess pore pressures at points P1 and P3 in model C80 under horizontal shaking and combined horizontal-vertical shaking.

reduced shaking.

3.2. *Effect of structural configuration*

The caisson in model C80H experiences slightly larger sinking (20 cm) than the caisson in model C80 (18 cm) while negligible horizontal displacement and rotation of the foundation can be observed in this case (see, Table 3). Fig. 18 illustrates the deformed shape of the soil in model C80H and corresponding displacement vectors at the end of the earthquake which clearly show the downward sinking of the foundation. From these results, it might be concluded that manifolds with larger height-to-width ratios can experience more settlements during liquefaction while less rotation and sliding displacements of the foundation may occur. This could partly be due to the larger natural period in rocking for a taller manifold, and therefore this response feature depends also on the characteristics of the earthquake shaking.

3.3. *Effect of thickness of liquefiabe layer*

The computed earthquake-induced displacements of the mudmat in model M150S, where it rests on a shallow liquefiable sand layer, were very close to those in model M150 indicating that the thickness of the liquefiable sand layer might not a governing factor on the seismic response of the foundation. Considering these results, it can be concluded that mudmats might experience almost the same level of sinking in both shallow and deep liquefiable sand during earthquake.

3.4. *Effect of bi-directional shaking*

The common practice in earthquake analyses of most structures is the application of only one component of the horizontal excitation. In some cases, the analyses are performed separately in three directions (two horizontal and one vertical), and the response of

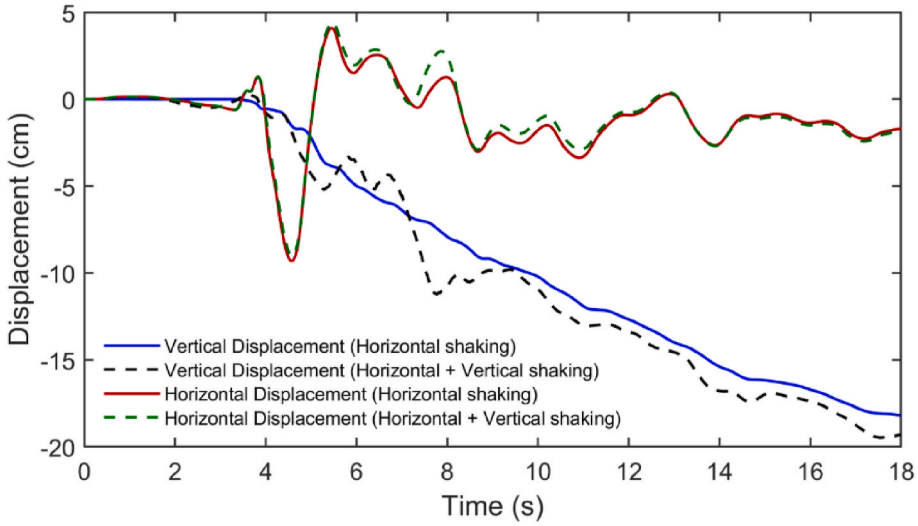

Fig. 20. Comparison of vertical displacements of caisson at point D2 in model C80 under horizontal shaking and combined horizontal-vertical shaking.

the structure is computed by combining these individual responses in a way (often specified by design codes) to account for the fact that the three responses are independent of one another. An attemptwas made in this study to investigate the impact of simultaneous horizontal and vertical excitation for one of the models. A concurrent horizontal excitation in the transverse direction was avoided because it would require a much larger model as the symmetry condition cannot be used and the model size in the transverse direction had to be extended. The horizontal transverse shaking would not change the liquefaction development and could, at most, increase the lateral movement of the structure by a few percent without affecting the overall conclusions.

Model C80 (Table 1) was used for the bi-directional analyses. Fig. 19 shows the simulated time histories of excess pore-water pressures at four depths for the cases with and without the vertical shaking. As the plots in this figure illustrate, the vertical shaking induces high-frequency oscillations in the pore-pressure values which quickly die out as the vertical shaking stops and the pore pressures simply follow the case with only horizontal shaking. It is interesting that these high-frequency oscillations have practically only a minor effect on the structural response. This is displayed by the plots in Fig. 20 which compare the horizontal and vertical displacements of the foundation for the cases of one-directional and bi-directional shakings. This observation has useful practical implications as it suggests that one could exclude the bi-directional shaking in such applications.

4. Conclusion

The liquefaction response of mudmat and caisson foundations for manifolds under various seismic loading conditions has been studied in this paper. To evaluate the performance of these foundations and to compare the results for different cases, excess pore water pressure and shear stress-strain responses in the soil medium together with the earthquake-induced displacements of the foundations have been computed and presented.

The excess pore pressure inside the caissons is lower than outside. This is believed to be due to kinematic confinement provided by the skirt of the foundation. When the excitation is strong enough, the sand liquefies at most points around the subsea foundations. Similar pore pressure patterns and final excess pore pressure ratios was observed due to both earthquake shakings considered in this study.

The numerical results indicate that considerable downward movements of the subsea foundation could occur during liquefaction and that the foundation can experience some additional post-liquefaction settlements due to soil consolidation. In general, caissons tend to undergo larger settlements during liquefaction mainly due to their higher weights and the mechanism of load transfer to the soil. Additionally, the permanent lateral displacements and rotations are small for typical earthquake motions and symmetrical manifolds, and as long as the vertical displacements (sinking) are acceptable for the performance of the manifold, it should be possible to accommodate the permanent lateral movements. Moreover, caissons, in general, tend to experience larger rotations than mat foundations. According to the simulated results, the thickness of the liquefiable soil layer and the concurrent vertical shaking have generally minor effects on the overall response of subsea foundations.

Declaration of competing interest

The authors declare that they have no known competing financial interests or personal relationships that could have appeared to influence the work reported in this paper.

References

[1] Kaynia AM. Earthquake geotechnics in offshore engineering. In: Recent advances in earthquake engineering in europe. Springer; 2018. p. 263–88.
[2] White DJ, Maconochie AJ, Cheuk CY, Bolton MD, Joray D, Springman SM. An investigation into the vertical bearing capacity of perforated mudmats. In: Proceedings of the 1st international symposium on frontiers in offshore geotechnics. ISFOG; 2005. p. 459–65.
[3] Tjelta TI, Haaland G. Novel foundation concept for a jacket finding its place. Offshore Site Investigation and Foundation Behaviour 1993;28:717–28.
[4] Bransby MF, Randolph MF. Combined loading of skirted foundations. Geotechnique 1998;48(5):637–55. https://doi.org/10.1680/geot.1998.48.5.637.
[5] Randolph MF, Erbrich CT. Design of shallow foundations for calcareous sediments. In: Al-Shafei KA, editor. Proceedings of the 2nd international conference on engineering for calcareous sediments; 1999. p. 361–78. Balkema (2).
[6] Gourvenec S, Randolph MF. Effect of strength non-homogeneity on the shape and failure envelopes for combined loading of strip and circular foundations on clay. Geotechnique 2003;53(6):575–86. https://doi.org/10.1680/geot.2003.53.6.575.
[7] Feng X, Randolph MF, Gourvenec S, Wallerand R. Design approach for rectangular mudmats under fully three-dimensional loading. Geotechnique 2014;64(1):51–63. https://doi.org/10.1680/geot.13.P.051.
[8] Shen Z, Feng X, Gourvenec S. Effect of interface condition on the undrained capacity of mudmats under six-degree-of-freedom loading. Geotechnique 2016;67(4):1–12. https://doi.org/10.1680/jgeot.16.P.097.
[9] Gourvenec S, Feng X, Randolph MF, White DJ. A toolbox approach for optimizing geotechnical design of subsea foundations. In: Proceedings of offshore technology conference; 2017. Houston, Texas.
[10] Doherty J, Krisdani H, O'Neil M, Erbrich C, Bransby MF, White D, Randolph M. The design of subsea foundations subjected to general cyclic loading using a massively scalable web based application. In: Proceedings of offshore technology conference; 2018. Houston, Texas.
[11] Kaynia AM, Dimmock P, Senders M. Earthquake response of pipelines on submarine slopes. In: Proceedings of offshore technology conference; 2014. Houston, Texas.
[12] Brennan AJ, Madabhushi SPG, Cooper P. Dynamic centrifuge testing of suction caissons in soft clay. In: Proceedings of the 6th international conference on physical modelling in geotechnics; 2006. p. 625–30.
[13] Ardoino F, Traverso CM, Parker EJ. Non-linear dynamic response of deepwater suction pile foundation. In: Geotechnical earthquake engineering and soil dynamics IV congress 2008, vol. 181; 2008.
[14] Memos CD, Kiara A, Pavlidis E. Coupled seismic response analysis of rubble-mound breakwater. In: Proceedings of the institution of civil engineers: water and maritime engineering, vol. 156; 2003. p. 23–31. 1.
[15] Ye J, Wang G. Seismic dynamics of offshore breakwater on liquefiable seabed foundation. Soil Dynam Earthq Eng 2015;76:86–99.
[16] Ye J, Huang D, Wang G. Nonlinear dynamic simulation of offshore breakwater on sloping liquefied. Bull Eng Geol Environ 2016;75(3):1215–25.
[17] Ye J, Huang D, Wang G. Numerical simulation of the seismic liquefaction mechanism in an offshore loosely deposited seabed. Bull Eng Geol Environ 2016;75(3):1183–97.
[18] Najma A, Ghalandarzadeh A. Experimental study on the seismic behavior of composite breakwaters located on liquefiable seabed. Ocean Eng 2019:186.
[19] Liang Z, Jeng DS, Liu J. Combined wave–current induced seabed liquefaction around buried pipelines: design of a trench layer. Ocean Eng 2020:212.
[20] Zhou X-L, Wang J-H, Zhang J, Jeng D-S. Wave and current induced seabed response around a submarine pipeline in an anisotropic seabed. Ocean Eng 2014;75:112–27.
[21] Erbrich CT, Wallbridge P, Yamamoto N. Numerical modelling of seismically induced settlement for Ichthys riser support structure. In: Offshore technology conference asia 2016; 2016. p. 3067–86.
[22] Younan AH, Kaynia AM, Loo MM, Widianto Khalifa J. Seismic design of Hebron platform - an integrated soil-structure-interaction approach. In: Proceedings of international conference on offshore mechanics and arctic engineering. Canada: Newfoundland; 2015.
[23] Wolf JP. Foundation vibration analysis using simple physical models for foundations dynamic. In: Proceedings of the 3rd international conference on recent advances in geotechnical earthquake engineering and soil dynamics; 1995. Missouri.
[24] Liingaard M. Dynamic behaviour of suction caissons [Ph.D. Dissertation]. Department of Civil Engineering, Aalborg University; 2006.
[25] Brandt M. Earthquake analysis of subsea structure on caisson foundation using 3D finite element solution. Department of Civil and Transport Engineering, Norwegian University of Science and Technology; 2014 [Msc Thesis].
[26] Zheng BL, Kutter BL, Hirt GS, Zhou YG, Wilson DW, Clukey EC. Centrifuge modeling of seismic behavior of caisson-supported subsea manifold on soft clay. In: The 6th international conference on earthquake geotechnical engineering; 2015. Christchurch.
[27] Stensløkken A. Study of the effect of added soil mass on earthquake response of subsea structures on closed caisson foundations. Department of Civil and Transport Engineering, Norwegian University of Science and Technology; 2016 [Msc Thesis].
[28] Athanasiu C, Bye A, Tistel J, Ribe A, Arnesen K, Feizikhanhandi S, Sørlie E. Simplified earthquake analysis for wind turbines and subsea structures on closed caisson foundations. In: Frontiers in offshore geotechnics III; 2015. Oslo.
[29] Kaynia AM. Seismic considerations in design of offshore wind turbines. Soil Dynam Earthq Eng 2018. https://doi.org/10.1016/j.soildyn.2018.04.038.
[30] Kaynia AM. Simple model for dynamic stiffness of underwater foundations. In: Proceedings of 2nd international conference of earthquake geotechnical engineering; 1999. p. 449–54. Lisbon, Portugal.
[31] Park J, Kaynia AM. Stiffness matrices for fluid and anisotropic soil layers with applications in soil dynamics. Soil Dynam Earthq Eng 2018;115:169–82. https://doi.org/10.1016/j.soildyn.2018.06.030.
[32] Cuéllar P, Mira P, Pastor M, Fernández-Merodo JA, Baeßler M, Rücker W. A numerical model for the transient analysis of offshore foundations under cyclic loading. Comput Geotech 2014;59:75–86.
[33] Corciulo S, Zanoli O, Pisano F. Transient response of offshore wind turbines on monopiles in sand: role of cyclic hydro–mechanical soil behavior. Comput Geotech 2017;83:221–38.
[34] Yang CB, Wang R, Zhang JM. Seismic analysis of monopile supported offshore wind turbine. In: International conference on geotechnical and earthquake engineering; 2018. Chongqing, China.
[35] Kementzetzidis E, Corciulo S, Versteijlen W G, Pisanò F. Geotechnical aspects of offshore wind turbine dynamics from 3D non-linear soil-structure simulations. Soil Dynam Earthq Eng 2019;120:181–99. https://doi.org/10.1016/j.soildyn.2019.01.037.
[36] Zhu B, Byrne BW, Houlsby GT. Long term lateral cyclic response of suction caisson foundations in sand. Journal of Geotechnical and Geoenvironmental Engineering, ASCE 2013;139(1):73–83.
[37] Kourkoulis RS, Lekkakis PC, Gelagoti FM, Kaynia AM. Suction caisson foundationsfor offshore wind turbines subjected to wave and earthquake loading: effect of soil foundation interface. Geotechnique 2014;64(3):171–85. https://doi.org/10.1680/geot.12.P.179.
[38] Kazemi Esfeh P, Kaynia AM. Numerical modeling of liquefaction and its impact on anchor piles for floating offshore structures. Soil Dynam Earthq Eng 2019;127. https://doi.org/10.1016/j.soildyn.2019.105839.
[39] Kazemi Esfeh P, Kaynia AM. Earthquake response of monopiles and caissons for Offshore Wind Turbines founded in liquefiable soil. Soil Dynam Earthq Eng 2020;136. https://doi.org/10.1016/j.soildyn.2020.106213.
[40] Biot MA. General theory of three-dimensional consolidation. J Appl Phys 1941;12(2):155–64. https://doi.org/10.1063/1.1712886.
[41] Kirkwood P, Dashti S. A centrifuge study of seismic structure-soil-structure interaction on liquefiable ground and implications for design in dense urban areas. Earthq Spectra 2018;34(3):1113–34. https://doi.org/10.1193/052417EQS095M.
[42] Dafalias YF, Manzari MT. Simple plasticity sand model accounting for fabric change effects. J Eng Mech 2004;130(6):622–34. https://doi.org/10.1061/(ASCE)0733-9399(2004)130:6(622).
[43] Ramirez J, Barrero A R, Chen L, Dashti S, Ghofrani A, Taiebat M, Arduino P. Site response in a layered liquefiable deposit: evaluation of different numerical tools and methodologies with centrifuge experimental results. J Geotech Geoenviron ASCE 2018;144(10). https://doi.org/10.1061/(ASCE)GT.1943-5606.0001947.